Physics in Medicine 7 (2019) 100016

Contents lists available at ScienceDirect

Physics in Medicine

journal homepage: www.elsevier.com/locate/phmed

Molecularly imprinted polymers to detect profenofos and carbofuran selectively with QCM sensors

Wongduan Sroysee[a,c], Suticha Chunta[b,c], Maliwan Amatatongchai[a], Peter A. Lieberzeit[c,*]

[a] Department of Chemistry and Center of Excellence for Innovation in Chemistry, Faculty of Science, Ubon Ratchathani University, Ubon Ratchathani, 34190, Thailand
[b] Faculty of Medical Technology, Prince of Songkla University, Songkla, 90110, Thailand
[c] University of Vienna, Faculty for Chemistry, Department of Physical Chemistry, 1090, Vienna, Austria

ARTICLE INFO

Keywords:
Molecularly imprinted polymer (MIP)
Quartz crystal microbalance (QCM)
Carbofuran (CBF)
Profenofos (PFF)

ABSTRACT

Two different molecularly imprinted polymers (MIP) were designed to selectively bind the insecticides carbofuran (CBF) and profenofos (PFF). CBF-MIP are based on methacrylic acid (MAA) as a functional monomer, ethylene glycol dimethacrylate (EGDMA) as a crosslinker, and azobisisobutyronitrile (AIBN) as an initiator. The PFF-MIP comprised of polyurethane based on poly (4-vinylphenol) (PVP), and diphenyl methane-4,4′-di-isocyanate (DPDI) as functional monomers, phloroglucinol (PG) as the cross-linker, and diphenylmethane (DPM) as the porogen. For sensor measurement, MIPs were spin-coated onto one electrode pair of a dual-electrode QCM, while the second pair was spin-coated with NIPs. Fourier transform infrared (FT-IR) spectroscopy confirms successful template removal from the polymer matrix. The resulting CBF- and PFF-MIP coated onto quartz crystal microbalances (QCMs) lead to pesticide QCM sensors revealing the following analytical characteristics, respectively: dynamic detection range of 0.5–1000 µM for CBF-MIP and 10–1000 µM for PFF-MIP. In both cases, the MIP exhibit roughly ten times higher sensor signals, than the corresponding non-imprinted polymers (NIP).

1. Introduction

Pesticides are used worldwide to destroy or control weeds, insects, fungi, and other pests in agriculture [1]. Their widespread application has resulted in residues in the environment, which pose inherent health risks to humans and mammals. The same is true for persons exposed to them while applying them. Nowadays, organophosphorus and organonitrogen pesticides have widely replaced organochloride compounds because of their low cost, comparably fast biodegradation, and low environmental toxicity [2,3]. Carbofuran (CBF) is an organonitrogen, and profenofos (PFF) an organophosphorus pesticide. Both are widely used to control insects. Despite the abovementioned advantages, these pesticides can still cause health conditions in humans, such as asthma attacks, skin rashes, and chronic neurological disorders [4]. Thus, it is necessary to detect and monitor their residues in farm products and in the environment.

So far, a range of analytical methods aiming at detecting CBF and PFF are available. They rely e.g. on spectrophotometry [5,6], or chromatography (HPLC, GC, GC/MS, and LC/MS-MS) [7–11]. Although these methods are sufficiently accurate, sensitive and specific, they still require expensive instrumentation and skilled analysts. Immunological methods, such as enzyme-linked immunosorbent assay (ELISA), have also been reported including real sample applications [12]. However, biological materials - i.e. antibodies, antigens and enzymes – are of limited use, because they are inherently costly and comparably sensitive towards environmental factors [12]. Those limitations have prompted development of synthetic selective receptors.

Molecularly imprinted polymers (MIP) have attracted substantial interest in this regard. MIPs are usually synthesized through co-polymerization of functional and cross-linking monomers in the presence of a template. The latter interacts with functional groups to form non-covalent [13], or covalent [14] bonds. MIP are suitable coatings for QCM to yield sensors with enhanced performance, such as high specificity, low cost, ease of use and rapidness of detection [15]. There are several successful reports on insecticide detection with molecularly imprinted polymers on QCM: For example, Gao et al. synthesized MIP using methacrylic acid (MAA) for recognition of PFF by physical entrapment and *in situ* self-assembly [16]. However, they carried out all measurements in gas phase. Ozkutuk and coworkers prepared MIP using methacryloyl chloride as the monomer to detect paraoxon [17]. Findeisen et al. synthesized MIP based on poly-4-vinylphenol as a monomer to detect dimethyl methylphosphonate (DMMP) [18], which seems a good starting point for PFF MIP. Successfully creating recognition sites depends on appropriately selecting all polymer

* Corresponding author.
E-mail address: peter.lieberzeit@univie.ac.at (P.A. Lieberzeit).

https://doi.org/10.1016/j.phmed.2019.100016
Received 31 January 2019; Received in revised form 27 February 2019; Accepted 7 March 2019
Available online 17 June 2019

constituents including functional monomers, template, solvent, cross-linker, and initiator. There are also examples of MIP sensors toward carbofuran [19] and profenofos [20], respectively. However, the former relies on electropolymerized systems and the latter on fiber-optical detection. To the best of our knowledge there are no acrylate- or urethane-based MIP for CBF and PFF, respectively, in literature that serve as receptors on QCM sensors. The rationale behind using those two systems is twofold: First, larger numbers of functional monomers are available in both cases, which makes it feasible to fine-tune interaction sites to optimally interact with PFF and CBF, respectively, e.g. by forming hydrogen bonds. Second, functional monomers are commercially available in a highly cost-effective way and can be polymerized conveniently on various substrate materials.

2. Experimental

2.1. Chemicals

Methacrylic acid (MAA), ethylene glycol dimethacrylate (EGDMA), 2,2′-azobisisobutyronitrile (AIBN), phloroglucinol (PG) and diphenyl methane 4,4′-di-isocyanate (DPDI) were purchased from Merck AG (Darmstadt, Germany) in highest available purity. Carbofuran (CBF, 98%), profenofos (PFF, 97.6%), chlopyrifos (CPF, ≥98%), poly(4-vinyl phenol) (PVP) and diphenyl methane (DPM) were obtained from Sigma – Aldrich (St. Louis, MO, USA).

2.2. Apparatus

Fourier transform infrared (FT-IR) spectra were recorded on a PerkinElmer Spectrum 100 in the range 4000-600 cm^{-1}. Quartz crystal microbalances (QCM) were based on AT-cut quartz with 14 mm diameter and a thickness of 168 µm comprising electrodes screen printed onto their surfaces by a process developed in the group [21]. Morphologies of CBF-MIP, PFF-MIP and the corresponding NIP films were evaluated by AFM using a scanning microscope probe (Park Systems Corp., Korea.) controlled by XEI software.

2.3. Synthesis of molecularly imprinted polymers and non-imprinted polymers

Two different types of MIP toward CBF and PFF, respectively, were prepared by free radical polymerization in a bulk imprinting approach as summarized in Scheme 1: For CBF-MIP synthesis, 15 µL (0.20 mmol) MAA as a functional monomer and 22.2 mg (0.10 mmol) CBF were dissolved in 600 µL DMSO in an Eppendorf tube. Then 25 µL (0.13 mmol) EGDMA as the cross-linker and 2.4 mg (0.02 mmol) AIBN as initiator were added and the mixture ultrasonicated for 10 min. Then, the solution pre-polymerized in a water bath at 70 °C until reaching the gel point while continuously stirring. Polymerization took place in Argon atmosphere to ensure oxygen-free conditions and thus minimal side reactions. After this, 4 µL of the resulting oligomer solution was dropped onto the surface of bare gold electrode of a QCM and spin-coated at 2000 rpm for 30 s. The NIP was prepared and spin-coated in the same way, but without adding CBF. Finally, MIP and NIP coatings were polymerized overnight by exposing to UV light with $\lambda^{max} = 312$ nm.

PFF-MIP was prepared by dissolving 59 mg (5.4 µmol) PVP (please note that this compound is a polymer, hence the low molar amount), 41 mg (0.16 mmol) DPDI, 8 mg PG, 10 mg (0.06 mmol) DPM, and 37.4 mg (0.10 mmol) PFF in 600 µL THF in an Eppendorf tube. The mixture was ultrasonicated for 10 min followed by pre-polymerizing in water bath at 75 °C for 3 h under Argon atmosphere. After that, 500 µL of THF was immediately added to the pre-polymer solution to stop the reaction. Before spin coating, the reaction mixture was diluted again with THF (1 part reaction mixture + 1 part solvent) to achieve thin films [18]. NIP resulted from the same procedure, but without adding PFF. Finally, the MIP and NIP solutions were spin-coated onto each of a QCM electrode pair at 3000 rpm for 1 min. The coated electrodes were hardened at room temperature overnight and then completely polymerized in a drying oven at 120 °C for 10 min.

Finally, the templates (CBF and PFF, respectively) were removed by immersing the respective QCM into a solvent mixture consisting of methanol and acetic acid (9:1 %v/v) for 30 min followed by deionized water for 30 min, respectively. Washing steps continued until network analyzer tests revealed constant resonance frequencies.

FT-IR spectroscopy was used for assessing the synthesized materials. MIP and NIP examined this way were prepared exactly in the same way as already described, but using glass slides as the substrate rather than QCM. After that, the MIP and NIP films were mechanically removed from glass slides, and mixed homogenously with KBr (samples: KBr = 1:200, w/w) in a mortar. Then MIP and NIP were pressed under hydraulic pump to form the KBr pellet.

2.4. Sensor measurements

Scheme 2 illustrates the setup of MIP-QCM detection system. Dual channel QCMs were custom-made by screen printing Brilliant gold paste onto the surface of quartz blanks. Screen printed QCM were heated to 400 °C for 4 h to remove organic residues and expose bare gold. QCM measurements followed previously published protocols [22]: A dual-channel QCM containing both MIP and NIP was installed into custom-made PDMS cell and connected to an oscillating circuit monitored by means of an Agilent HP5313A frequency counter. Measurements were carried out in stopped-flow mode. For that purpose, the sensor chamber was first flushed with deinoized water. The frequency reached at equilibrium defined the base line for the measurement. After this, we injected a solution containing the respective pesticide in deionized water and waited for equilibrium again. Corresponding data was read out into computer through Agilent GPIB interface with LabView software. Finally, we flushed out samples by flowing water over the sensor surfaces until reaching equilibrium signal.

3. Results and discussion

3.1. FT-IR characterization of MIP and NIP

Fig. 1a and Fig. 1b summarize the FT-IR spectra taken after different steps of synthesizing CBF-MIP and PFF-MIP, respectively. It shows the NIP and the MIP before, and after removing the template, respectively. The FT-IR spectrum of CBF-MIP (Fig. 1a) before template removal shows a peak at 3355 cm^{-1} attributed to N–H stretching from CBF molecules that adsorb in the polymer layer synthesized from MAA: CBF N–H groups have the ability to form strong hydrogen bonds, e.g. with monomers. At the same time, CBF-MIP after template removal and NIP films do not contain this spectral band, which strongly indicates that the template had been removed successfully. However, both spectra reveal an OH stretching band around 3425 cm^{-1} that can be associated with carboxylic group (COOH) of MAA. All PFF-MIP spectra in Fig. 1b show absorption bands of N–H originating from PVP at 3329 cm^{-1}, i.e. it is visible in MIP before and after removing the template, and NIP. The PFF-MIP before template removal reveals PFF absorption bands at 1464, 1150, 949, 682 and 628 cm^{-1} for C–H, P═O, P–S, C–Cl, and C–Br respectively. Neither of these spectral bands is visible in MIP spectra after removing PFF, and NIP, respectively. This is strong evidence that PFF is absent in both of them presumably leading to recognition sites in the material as outlined in Scheme 1. These results indicate successful PFF and CBF removal from the corresponding MIPs and the formation of imprinted sites at the polymer layer. This is in line with previous work [23,24].

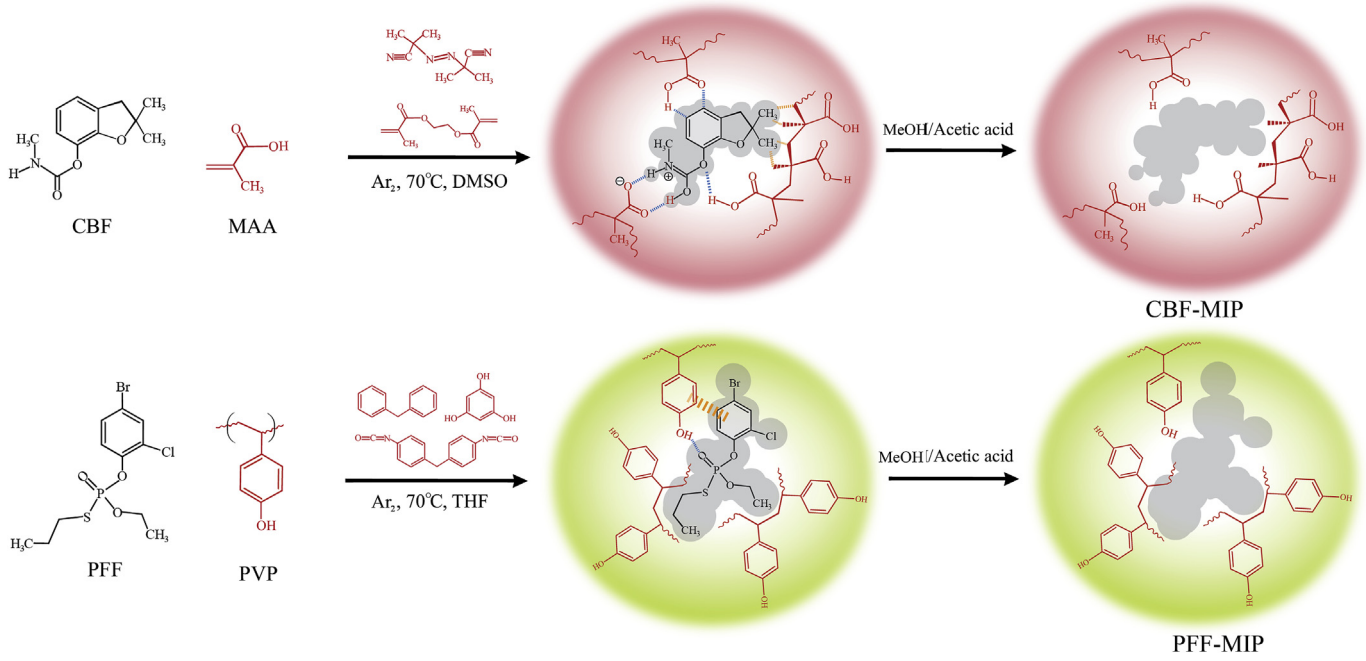

Scheme 1. Synthesis approach to CBF-MIP (A), and PFF-MIP (B).

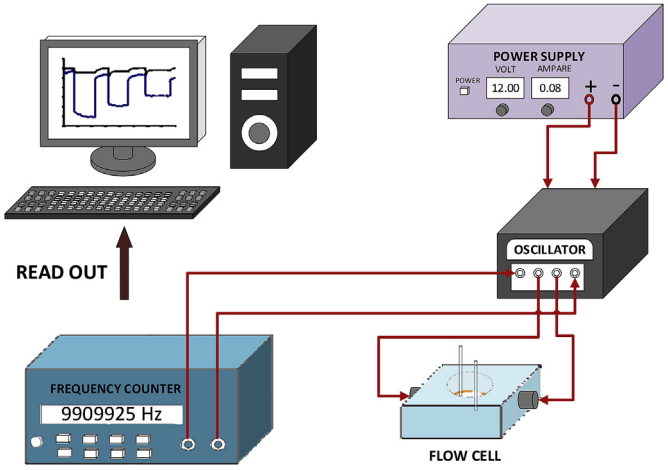

Scheme 2. Setup of MIP-QCM detection system.

3.2. AFM characterization

The surfaces of MIP after removing the template and NIP were characterized using AFM (5 μm × 5 μm scan size) in contact mode with NP-S10 silicon nitride tips by Bruker metrology. Fig. 2a–b shows AFM images of polymers template by CBF and PFF, respectively. As shown in Fig. 2a, the morphologies of CBF-MIP after template removal displays a large number of spherical structures and cavities whereas the NIP shows comparably smooth surface. Fig. 2b shows the significant difference between PFF-imprinted and non-imprinted films. PFF-MIP after the template removal exhibits larger surface roughness compared to NIP. The MIP after the template removal reveal cavities on the surface, which are not present in the NIP. This clearly demonstrates that the morphology of MIP thin films differs from their non-imprinted counterparts. Of course it is not possible of visualize individual imprints, because lateral resolution of AFM is determined by tip aperture, which is 5–10 nm in this case. It still clearly demonstrates that molecular imprinting also has some overall effect on the corresponding polymer. The thicknesses of PFF-MIP and CBF-MIP thin films were measured revealing 20 and 80 nm height, respectively. For that purpose, each

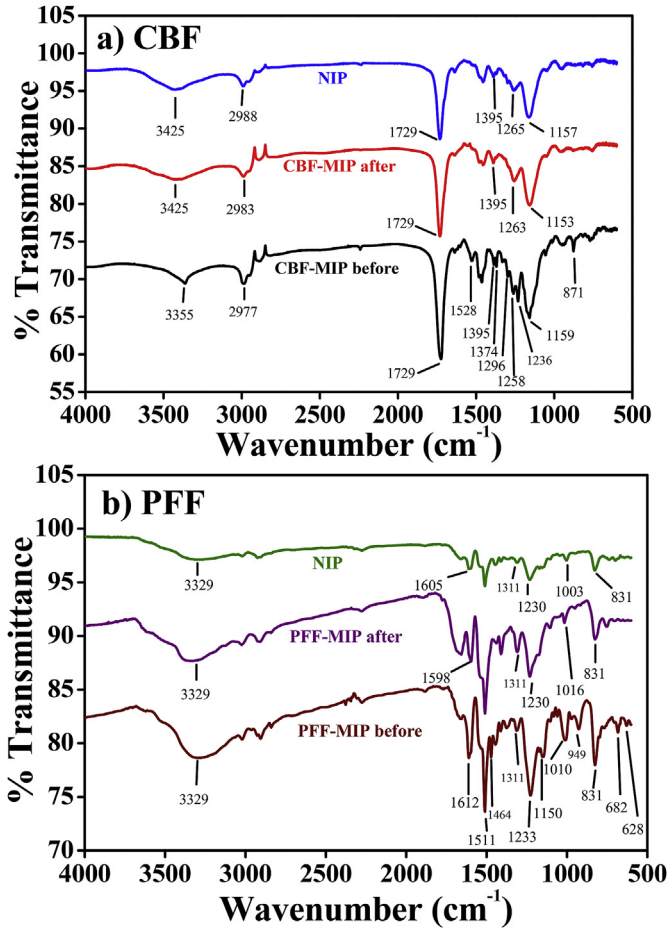

Fig. 1. FT-IR spectra of CBF-MIP (a) and PFF-MIP (b).

electrode was characterized by the means of a network analyzer before and after coating and after removing the template. Observed frequency shifts depend on mass. The respective relation between mass change

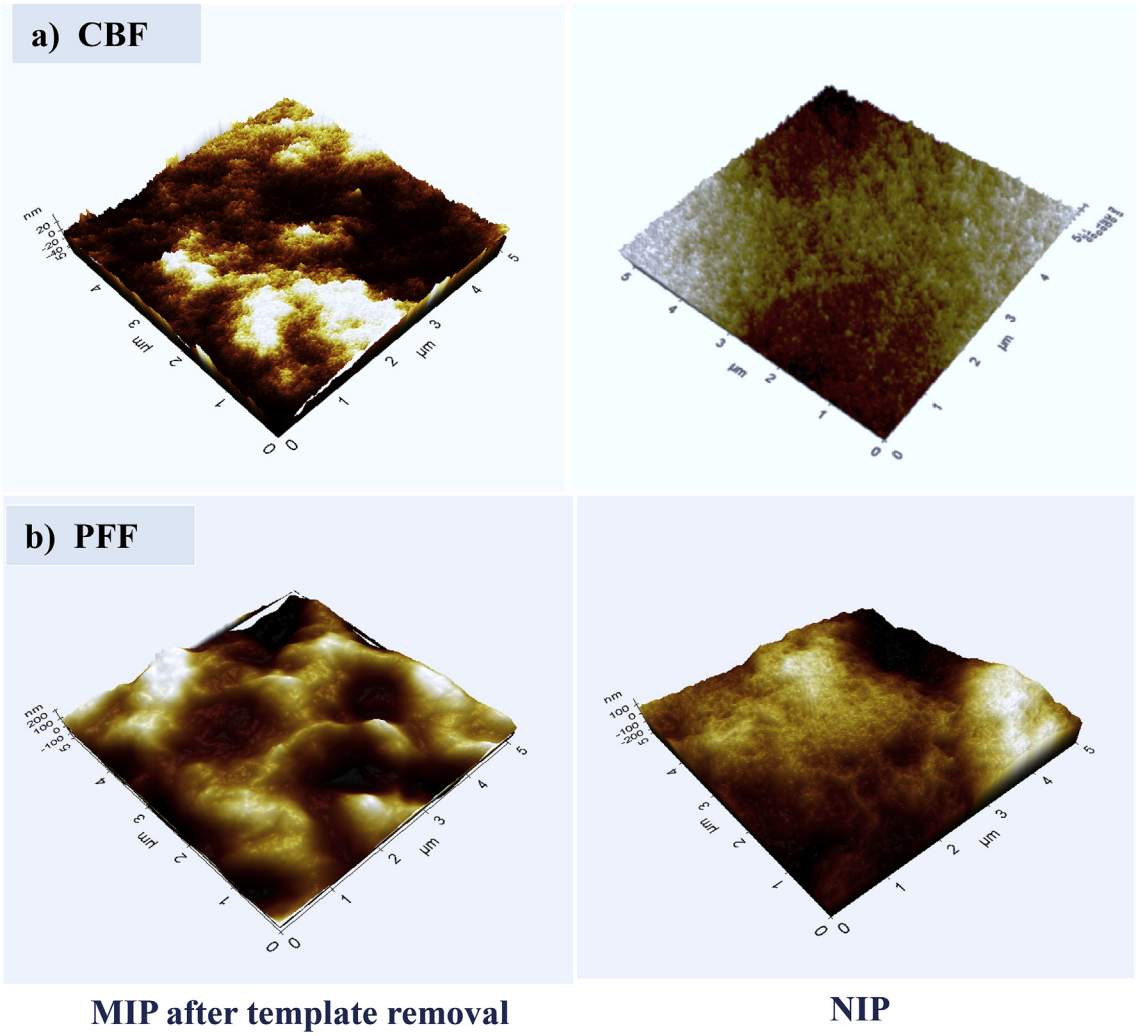

Fig. 2. AFM image of CBF-MIP (a) and PFF-MIP (b) and corresponding NIP on glass slides.

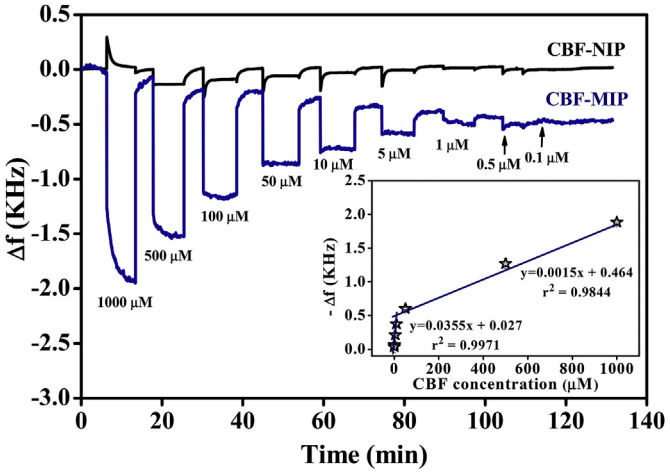

Fig. 3. QCM sensor responses toward CBF at various concentrations; the inset shows bi-linear sensor characteristic in the concentration range of 0.5–1000 µM.

Δm and frequency shift (ΔF), is given in Eq. (1) [24].

$$\Delta F = \frac{-2F_0^2}{A\sqrt{\rho u}}\,\Delta m \tag{1}$$

where ΔF is the measured frequency change (Hz), F_0 the fundamental frequency of QCM (6×10^6 Hz), Δm the mass change (g), A the electrode area 1.33 cm^2, ρ the density of quartz (2.65 g/cm^3) and μ is the shear module of quartz (2.95×10^{11} dyn/cm^2). Inserting the respective values into the Sauerbrey equation and assuming that the density of the polymer is $\rho = 1\ g/cm^3$ leads to the conclusion that $\Delta F = -1$ kHz corresponds to 40 nm layer height [25].

3.3. Sensitivity

The rationale for choosing MAA and PVP as functional monomers for CBF-MIP and PFF-MIP, respectively, is to interact strongly with the template by providing multiple ways of interaction such as H-bond donor, H-bond receptor, dipole-dipole interaction and van der Waals interaction based on literature [26]. CBF and PFF are comparably large templates for bulk molecular imprinting. Therefore, choosing the proper eluent is important to make sure to remove the template efficiently from the polymer matrix. A solvent mixture comprising methanol and acetic acid (9:1 %v/v) was chosen, because methanol can be used to break hydrogen bonding between template and binding sites, while acetic acid is believed to compete with the template for functional groups in the binding site [27,28]. Then, the frequency shifts ($F_0 - F_1$) were calculated, resulting 1850 Hz and −644 Hz for PFF-MIP and CBF-MIP, respectively.

Fig. 3 shows the QCM sensor responses of CBF-MIP in comparison with CBF–NIP, which acted reference. CBF-MIP leads to substantial

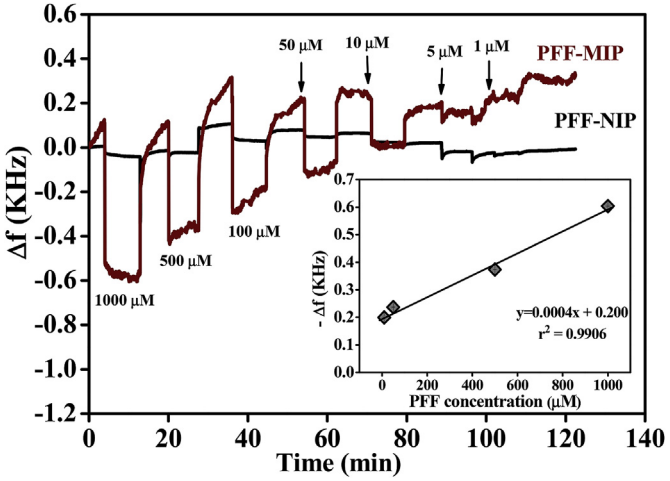

Fig. 4. QCM responses toward different concentration of PFF; The insert shows linear sensor characteristic in the concentration range of 5–1000 µM.

frequency signals in a range of 50–1850 Hz. In contrast, the NIP-coated electrode yields slightly positive frequency shift in the range of 13–130 Hz. MIP signals are thus substantially larger, namely around 10 times, than those for the NIP. The reason is that the –NH group of CBF can interact with the –COOH functionality of the polymer backbone. This result is in line with previous reports by *Kotova* et al. [25] on detecting ephedrine with MIP. The inset of Fig. 3 shows the corresponding sensor characteristic: it contains two linears in the concentration ranges of 5–10 µM and 10–1000 µM, respectively.

Fig. 4 shows typical frequency responses of PFF-MIP and PFF-NIP toward solutions containing different concentrations of this analyte. Obviously, PFF gave rise to sensor signals as high as −644 Hz and −74 Hz for MIP and NIP, respectively, when using 1 mM solutions. The frequency shift of the MIP in this case is seven times higher than that of the NIP, the latter allowing for assessing affinity interaction between PFF and the respective polymer matrix. However, slight drift of the baseline can be seen on the PFF-MIP-coated electrode. This phenomenon does not influence the recognition ability of the system, but may be the consequence of the fact that damping on the MIP electrode made it more difficult to stabilize the oscillator circuit. This circumstance is consistent with previous work [25] and can be regarded a technicality. PFF-MIPs display linear working range from 5 to 1000 µM. The limit of detection (LOD) was found to be about 0.21 µM and 0.38 µM (S/N = 3) for CBF-MIP and PFF-MIP, respectively. Table 1 compares the proposed sensors (CBF-MIP and PFF-MIP) with previously published methods. Notably, the performance of proposed electrode is comparable or even better than that of the previous reported QCM sensors for CBF and PFF detection. Besides, this method also provides a very convenient approach determining these analytes.

Based on the sensor characteristics of CBF-MIP and PFF-MIP, respectively, we then determined the corresponding binding isotherms. For that purpose, we applied a Langmuir adsorption isotherm model, as stated in Eqn. (2) [33,34]:

$$\Delta m = \frac{\Delta m_{max}}{K_d + C} \tag{2}$$

Where Δm is amount of increased mass on unit area of QCM sensor (g/cm^2); Δm_{max} is maximum saturation binding value; C is concentration of CBF or PFF solution (µM) for CBF-MIP or PFF-MIP, respectively; K_d is reverse binding constant equal to the inverse of the equilibrium association constant. For any given mass deposition, the respective isotherm parameters can be according to equation (3).

$$\Delta m = \frac{\Delta m_{max} \times K_a C}{1 + K_a} \tag{3}$$

For practical reasons, Eqn. (3) is usually rearranged to Eqn. (4): This allows for plotting Δm versus Δm/C which yields the slope of $1/K_a$ and Y-intercept of Δm_{max}.

$$\Delta m = -\frac{1}{K_a} \times \frac{\Delta m}{C} + \Delta m_{max} \tag{4}$$

Where K_a is forward binding constants. All masses were calculated from the frequency shifts according to the Sauerbrey equation [35]. The free energy change (ΔG) value for CBF and PFF adsorbed on the MIP-CBF and PFF-MIP immobilized QCM were calculated according to the following Eqn. (5) [24].

$$\Delta G = -RT \times \ln K_a \tag{5}$$

Where R is gas constant (8.314 J mol^{-1} K^{-1}), T (K) is the temperature.

Table 2 summarizes the results: CBF-MIP contains two K_a of 0.1 and 0.01 μM^{-1} for low and high concentration ranges of CBF, respectively. The rapid increase at low CBF concentrations correlates to the presence of large number of vacant imprinted cavities of MIP. Subsequently, these cavities re-bind template molecules leading to decreasing adsorption rate at higher concentrations. In case of PFF-MIP, K_a and Δm_{max} were 0.13 μM^{-1} and 3.03 g, respectively. This reveals strong affinity of PFF-MIP toward its analyte.

Table 2 also lists the corresponding Gibbs Energies for binding ΔG clearly revealing spontaneous binding.

The reproducibility of measurements for CBF-MIP and PFF-MIP were evaluated by measuring the same concentrations for 3 times. The calculated relative standard deviations (RSD) are 4.15% and 5.32% for CBF-MIP and PFF-MIP, respectively. These results point out that our method provides satisfactory reproducibility.

Table 1
Comparison of the proposed sensor with the previous methods towards the sensing of CBF and PFF.

Electrodes	Detection techniques	Monomer	Detection limit (µM)	Ref.
CBF				
AuNPs-MIP/GCE	DPV	ABA	0.024	[29]
GO@AuNPs-MIP/GCE	DPV	MAA	0.02	[19]
NiOPc-GO/CPE	Amperometry	–	1.7	[30]
anti-carbofuran IgG/Au	QCM	–	4.5	[31]
CBF-MIP/Au	QCM	MAA	0.21	This work
PFF				
MIP/Au	SPR	MAA	9.6×10^{-4}	[32]
MIP/Au	QCM	MAA	5.36×10^{-4}	[16]
PFF-MIP/Au	QCM	PVP	0.38	This work

AuNPs = gold nanoparticles, GO = graphene oxide, NiOPc = nickel (II) 1,4,8,11,15,18,22,25-octabutoxy-29H, 31H-phthalocyanine, ABA = Aminobenzoic acid, MAA = methacrylic acid, PVP = poly (4-vinyl phenol), DPV = Differential pulse voltammetry, SPR = Surface plasmon resonance, GCE = glassy carbon electrode, CPE = carbon paste electrode, Au = gold electrode.

Table 2
Langmuir constants of CBF-MIP and PFF-MIP.

substrate	K_a (μM^{-1})	Δm_{max} (μg)	ΔG (KJ mol^{-1}) at 25 °C
CBF-MIP	0.10	0.65	−5.70
	0.01	1.27	−11.41
PFF-MIP	0.13	306.91	−5.05

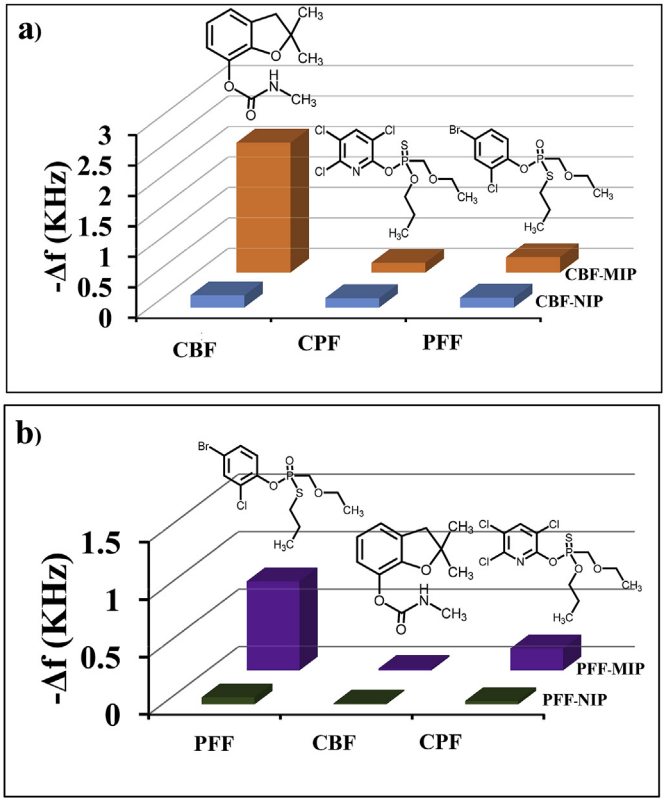

Fig. 5. Selectivity pattern of CBF-MIP and PFF-MIP, respectively, toward CBF, PFF and CPF at a concentration of 1000 μM.

Table 3
Selectivity of MIP sensor at 1000 μM of analyte and interferents.Table 1.

substrate	ΔF MIP (%)	ΔF NIP (%)	α	β
CBF-MIP				
CBF	83.89	38.88	2.15	1
CPF	6.22	30.03	0.21	10.42
PFF	9.89	31.09	0.32	6.78
PFF-MIP				
PFF	79.23	62.37	1.27	1
CPF	19.26	30.15	0.64	1.99
CBF	1.46	7.48	0.20	6.50

3.4. Selectivity

PFF and chlopyrifos (CPF) served to study the selectivity of CBF-MIP whereas CBF and CPF were selected for PFF-MIP. Fig. 5 shows responses of insecticide binding for CBF-MIP (a) and MIP-PFF (b) when exposed to solutions containing the respective pesticide at c = 1 mM. The frequency shifts of CBF-MIP and PFF-MIP were higher than those obtained from CBF–NIP and PFF-NIP, respectively. Furthermore, imprinting and selecting factors are defined as α and β shown Eq. (6) and Eq. (7) [19].

$$\alpha = \frac{\Delta F_{MIP}}{\Delta F_{NIP}} \quad (6)$$

$$\beta = \frac{\alpha_{MIP}}{\alpha_{analog}} \quad (7)$$

Where α is the imprinting factor (IF), which is defined as the ratio of frequency shift obtained from MIP and NIP; β is the selectivity coefficient, which was calculated from the ratio of imprinting factor obtained from analyte and analogue. Table 3 summarizes the results. The calculated α of analyte (CBF for CBF-MIP and PFF for PFF-MIP) were in the range of 0.20–2.15. Obviously, α values obtained from CBF-MIP and PFF-MIP higher than that obtained from competing compounds. The calculated β values were 10.42 (CPF) and 6.78 (PFF) for CBF-MIP and 1.99 (CPF) and 6.50 (CBF) for PFF-MIP. Overall, the results thus clearly demonstrate appreciable selectivity and sensitivity of the respective sensors.

4. Conclusion

In this work, we have developed two MIP sensors based on QCM targeting carbofuran and profenofos, respectively. They yielded linear ranges of 0.5–1000 and 5–1000 μM for CBF-MIP and PFF-MIP, respectively. The CBF-MIP and PFF-MIP detection limits are estimated to be 0.21 μM and 0.38 μM (S/N = 3), respectively. The results from selectivity studies demonstrated that the CBF-MIP and PFF-MIP provides acceptable selectivity for the determination of CBF and PFF, respectively.

Acknowledgment

This work was financially supported by grants from the Thailand Research Fund (TRF: RSA6080062) and the Center of Excellence for Innovation in Chemistry (PERCH-CIC), Office of the Higher Education Commission, Ministry of Education (OHEC). The authors are also grateful to the PhD. scholarship of the Science Achievement Scholarship of Thailand (SAST) and exchange scholarship of the University of Vienna, Faculty for Chemistry, Department of Physical Chemistry, Austria, given to W. Sroysee. Finally, authors gratefully acknowledge support by the ASEAN-European Academic University Network (ASEA-UNINET).

Appendix A. Supplementary data

Supplementary data to this article can be found online at https://doi.org/10.1016/j.phmed.2019.100016.

References

[1] G. Bapat, C. Labade, A. Chaudhari, S. Zinjarde, Silica nanoparticle based techniques for extraction, detection, and degradation of pesticides, Adv. Colloid Interface Sci. 237 (2016) 1–14.
[2] A.A. Bazrafshan, M. Ghaedi, Z. Rafiee, S. Hajati, A. Ostovan, Nano-sized molecularly imprinted polymer for selective ultrasound-assisted microextraction of pesticide carbaryl from water samples: spectrophotometric determination, J. Colloid Interface Sci. 498 (2017) 313–322.
[3] M. Tankiewicz, J. Fenik, M. Biziyk, Determination of organophosphorus and organonitrogen pesticides in water samples, Trends Anal. Chem. 29 (2010) 1050–1063.
[4] S. Liu, Z. Zheng, X. Li, Advances in pesticide biosensor: current status, and future perspectives, Anal. Bioanal. Chem. 405 (2013) 63–90.
[5] N. Chu, S. Fan, Sequential injection kinetic spectrophotometric determination of quaternary mixture of carbamate pesticides in water and fruit samples using artificial neural networks for multivariate calibration, Spectrochim. Acta, Part A 74 (2009) 1173–1181.
[6] W. Li, Y. Hua, S. Hong-Qing, W. Dan-Dan, Aptamer-based fluorescence assay for detection of isocarbophos and profenofos, Chin. J. Anal. 44 (2016) 799–803.
[7] Q. Wu, G. Zhao, C. Feng, C. Wang, Z. Wang, Preparation of a graphene-based magnetic nanocomposite for the extraction of carbamate pesticides from environmental water samples, J. Chromatogr., A 1218 (2011) 7936–7942.
[8] I. Machado, N. Gerez, M. Piston, H. Heinzen, M.V. Cesio, Determination of pesticide residues in globe artichoke leaves and fruits by GC–MS and LC–MS/MS using the same QuEChERS procedure, Food Chem. 227 (2017) 227–236.
[9] N.S. Pano-Farias, S.G. Ceballos-Magana, R. Muniz-Valencia, J.M. Jurado, A. Alcazar, I.A. Aguayo-Villarreal, Direct immersion single drop micro-extraction

method for multi-class pesticides analysis in mango using GC–MS, Food Chem. 237 (2017) 30–38.
[10] J.A. Ferreira, J.M.S. Ferreira, V. Talamini, J.F. Facco, T.M. Rizzetti, O.D. Prestes, M.B. Adaime, R. Zanella, C.B.G. Bottoli, Determination of pesticides in coconut (*Cocos nucifera* Linn.) water and pulp using modified QuEChERS and LC–MS/MS, Food Chem. 213 (2016) 616–624.
[11] P. Kaczynski, I. Hrynko, B. Lozowicka, Evolution of novel sorbents for effective clean-up of honeybee matrix in highly toxic insecticide LC/MS/MS analysis, Ecotoxicol. Environ. Saf. 139 (2017) 124–131.
[12] K. Zeng, T.B. Yang, P. Zhong, S.Y. Zhou, L. Qu, J. He, Development of an indirect competitive immune assay for parathion in vegetables, Food Chem. 102 (2007) 1076–1082.
[13] D.A. Spivak, K.J. Shea, Binding of Nucleotide based by imprinted polymer, Macromolecules 31 (1998) 2160–2165.
[14] M.J. Whitcombe, M.E. Rodriguez, P. Villar, E.N. Vulfson, A new method for the introduction of recognition site functionality into polymers prepared by molecular imprinting: synthesis and characterization of polymeric receptors for cholesterol, J. Am. Chem. Soc. 117 (1995) 7105–7111.
[15] S. Suriyanarayanan, P.J. Cywinski, A.J. Moro, G.J. Mohr, W. Kutner, Chemosensors based on molecularly imprinted polymers, Top. Curr. Chem. 325 (2012) 165–266.
[16] N. Gao, J. Dong, M. Liu, B. Ning, C. Cheng, C. Guo, C. Zhou, Y. Peng, J. Bai, Z. Gao, Development of molecularly imprinted polymer films used for detection of profenofos based on a quartz crystal microbalance sensor, Analyst 137 (2012) 1252–1258.
[17] E.B. Ozkutuk, S.E. Diltemiz, E. Ozalp, L. Uzun, A. Ersoz, Ligand exchange and MIP-based paraoxon memories onto QCM sensor, Appl. Phys. A 119 (2015) 351–357.
[18] A. Findeisen, J. Wackerlig, R. Samardzic, J. Pitkanen, O. Anttalainen, F.L. Dickert, P.A. Lieberzeit, Artificial receptor layers for detecting chemical and biological agent mimics, Sens. Actuators, B 170 (2012) 196–200.
[19] X. Tan, Q. Hu, J. Wu, X. Li, P. Li, H. Yu, X. Li, F. Lei, Electrochemical sensor based on molecularly imprinted polymer reduced graphene oxide and gold nanoparticles modified electrode for detection of carbofuran, Sens. Actuators, B 220 (2015) 216–221.
[20] A.M. Shrivastav, S.P. Usha, B.D. Gupta, Fiber optic profenofos sensor based on surface plasmon resonance technique and molecular imprinting, Biosens. Bioelectron. 79 (2016) 150–157.
[21] N.V.H. Phan, H.F. Sussitz, P.A. Liberzeite, Polymerization parameters influencing the QCM response characteristics of BSA MIP, Biosensors 4 (2014) 161–171.
[22] M. Hussain, N. Iqbal, P.A. Lieberzeit, Acidic and basic polymers for molecularly imprinted folic acid sensors—QCM studies with thin films and nanoparticles, Sens. Actuators, B 176 (2013) 1090–1095.
[23] B.H. Stuart, Infrared Spectroscopy: Fundamentals and Applications, John Wiley & Sons, Ltd, 2004, p. 84.
[24] M.E. Khalifa, I.M.M. Kenawy, Y.G. Abou El-Reash, A.B. Abdalla, Extractive separation of profenofos as an organophosphorous insecticide from wastewater and plant samples using molecular imprinted cellulose, J. Environ. Chem. Eng. 5 (2017) 3447–3454.
[25] K. Kotova, M. Hussain, G. Mustafa, P.A. Lieberzeit, MIP sensors on the way to biotech applications: targeting selectivity, Sens. Actuators, B 189 (2013) 199–202.
[26] G. Fang, Y. Yang, H. Zhu, Y. Qi, J. Liu, H. Liu, S. Wang, Development and application of molecularly imprinted quartz crystal microbalance sensor for rapid detection of metocarb in food, Sens. Actuators, B 251 (2017) 720–728.
[27] M.L. Mena, P. Martınez-Ruiz, A.J. Reviejo, J.M. Pingarron, Molecularly imprinted polymers for on-line preconcentration by solid phase extraction of pirimicarb in water samples, Anal. Chim. Acta 451 (2002) 297–304.
[28] M.M. Sanagi, S. Salleh, W.A.W. Ibrahim, a Ahmedy Abu Naim, D. Hermawa, M. Miskam, I. Hussain, H.Y. Aboul-Enein, Molecularly imprinted polymer solid-phase extraction for the analysis of organophosphorus pesticides in fruit samples, J. Food Compos. Anal. 32 (2013) 155–161.
[29] Q. Peipei, W. Jiao, W. Xiangyun, W. Zhiwei, X. Hao, D. Qiang, W. Xinguan, Sensitive and selective detection of the highly toxic pesticide carbofuran in vegetable samples by a molecularly imprinted electrochemical sensor with signal enhancement by AuNPs, RSC Adv. 8 (2018) 25334–25341.
[30] A. Wong, M.D. Pilar, T. Sotomayor, Determination of carbofuran and diuron in FIA system using electrochemical sensor modified with organometallic complexes and graphene oxide, J. Electroanal. Chem. 731 (2014) 163–171.
[31] K. Jia, P.-M. Adam, R.E. Ionescu, Sequential acoustic detection of atrazine herbicide and carbofuran insecticide using a single micro-structured gold quartz crystal microbalance, Sens. Actuators, B 188 (2013) 400–404.
[32] J. Dong, N. Gao, Y. Peng, C. Guo, Z. Lv, Y. Wang, C. Zhou, B. Ning, M. Liu, Z. Gao, Surface plasmon resonance sensor for profenofos detection using molecularly imprinted thin film as recognition element, Food Control 25 (2012) 543–549.
[33] M. Pan, Y. Gu, M. Zhang, J. Wang, Y. Yun, S. Wang, Reproducible molecularly imprinted QCM sensor for accurate, stable, and sensitive detection of enrofloxacin residue in animal-derived foods, Food Anal. Methods. 11 (2018) 495–503.
[34] G. Bayramoglu, M.Y. Arica, Development of a sensitive method for selection of affinity ligan for typsin using quartz crystal microbalance sensor, Bioproc. Biosyst. Eng. 35 (2012) 423–431.
[35] T. Kobayashi, Y. Murawaki, P.S. Reddy, M. Abe, N. Fujii, Molecular imprinting of caffeine and its recognition assay by quartz-crystal microbalance, Anal. Chim. Acta 435 (2011) 141–149.